On the Evaluation of the Intrinsic Stability of Indium-Nanoparticulate Organic Matter Complexes

Elise Rotureau, José-Paulo F Pinheiro, Jerome F. L. Duval

On the Evaluation of the Intrinsic Stability of Indium-Nanoparticulate Organic Matter Complexes

Elise Rotureau[1*], José Paulo Pinheiro[1], Jérôme F. L. Duval[1]

[1] Université de Lorraine, CNRS, Laboratoire Interdisciplinaire des Environnements Continentaux (LIEC), UMR 7360, Vandoeuvre-lès-Nancy, F-54000, France.

[*] Corresponding author : Elise Rotureau (elise.rotureau@univ-lorraine.fr)

Abstract

Hypothesis

Proper evaluation of the intrinsic stability of metals with humic nanoparticles calls for a robust representation of the particulate electrostatic features. Addressing here the case of trivalent metal association with humics for which a significant electrostatic contribution is expected, we report a robust interpretative approach as an alternative to the conventional but approximative Donnan model applied in the speciation codes.

Experiments

The intrinsic chemical binding affinity of Indium to humic nanoparticles is tackled from equilibrium electroanalytical measurements (Absence of Gradient and Nernstian Equilibrium Stripping) in $NaClO_4$ electrolyte (10-100mM, pH4) at different metal-to-humics concentration ratios. The electrostatic contribution was evaluated using a Poisson-Boltzmann based-approach where the key electrostatic descriptors of humics are involved.

Findings

The electrochemical results interpreted in the light of so identified non-specific indium binding contribution evidences a dramatic impact of electrostatics on indium complexation by humics, with *e.g.* in 10mM electrolyte an intraparticulate Boltzmann metal accumulation factor that is *ca.* 5 times larger than that reported for cadmium and highly-charged fulvics complexants. A successful comparison between theory and experiments is consistently achieved over the tested electrolyte concentrations with the only adjustment of the radius of the metal accumulation spherical volume. The analysis reveals the necessity to consider full equilibration of charged humics with its intraparticulate counterion atmosphere.

Keywords: Indium speciation; Trivalent cations; humic nanoparticles; intrinsic binding constants; AGNES; Poisson-Boltzmann electrostatics

INTRODUCTION

Humic substances are naturally occurring polyelectrolytic materials that significantly control the speciation of trace metals in soils and natural waters, their transport and toxicity towards biota [1]. Recent conceptual framework supported by measurements have evidenced that a comprehensive evaluation of the molecular processes underlying the complexation of metals by humic nanoparticles (HNP) in aquatic media is mandatory for addressing the stability of HNP-metal complexes [2–5], their kinetics of formation and dissociation (chemodynamics)[6–8] and their (bioavai)lability at reactive macroscopic biointerfaces like microorganisms [9,10]. The common feature between chemodynamic and thermodynamic descriptors of metal binding to HNP and, more generically, to any other charged nanoparticulate complexants, is that they both inherently depend on the physicochemical environment of the HNP body and of its close surrounding, *i.e.* the regions where actual metal complexation takes place and where metal transfer by conductive diffusion to/from the complexant is operational [7,11–13]. Under conditions where fully equilibrated metal speciation is achieved in HNP dispersions -which is subject to verification of the relevant dynamic criteria [14]- a clear connection must then be formulated between measurable (and apparent) stability constant of particulate metal complexes described in terms of metal and reactive site concentrations smeared-out over the whole sample volume, and that elaborated on the basis of relevant *local* intraparticulate concentrations of metal and reactant species [14]. This differentiation between *local* and *smeared-out* concentrations makes it possible to portray equilibrium metal speciation at the scale of an individual HNP complexant following practical strategies delineated by Town *et al.*[5] on the basis of *e.g.* electroanalytical measurements performed in 1-1 and 2-1 background electrolytes [2,3]. This leads, in particular, to evaluation of the fraction of intraparticulate hydrated free and inner-sphere complexed metal ions, and to quantitative appreciation of electrostatic metal condensation in the extra- or intra-particulate electric double layer regions [5].

Consistent recovery of intrinsic binding affinity of metals to HNP from experimental measurements is systematically tied to adequate modelling of the electrostatic potential distribution from bulk electrolyte solution to inner part of HNP body [2–5]. Within the equilibrium NICA-Donnan and WHAM/Model VII metal speciation concepts [15–18], this potential distribution is considered to obey *a priori* Donnan representation, regardless of the size of the particulate complexant compared to the Debye layer thickness. This approximation, if applied to HNP particles with radius *e.g.* lower than *ca.* 5 nm, comes to violate the fundamental electrostatic Poisson equation under practical conditions of solution ionic strengths (1 to 100 mM) [19]. Intrinsic chemical binding affinities derived with considering such inadequate electrostatic framework as a starting basis generally loses physicochemical significance [19]. This is reflected, in particular, by metal binding heterogeneity features that are inconsistent compared to those independently addressed from stripping electrochemical measurements [20,21]. The reader is referred to the critical review [19] of the NICA-

Donnan and WHAM/Model VII modelling framework for further details on the limits or incorrectness of their particle electrostatic descriptors. Accordingly, physically sound alternatives have been proposed, in agreement with experimental data, to better describe the extend and mode of electrostatic association of metals to soft and hard nanoparticulate ligands carrying reactive sites distributed in their volume (like HNP) or confined to their surface, respectively [14,22]. These alternatives are based on the governing Poisson-Boltzmann (PB) equation which captures the magnitude and structure of particle electric field operating in the extra- and/or intra-particulate regions depending on particle size, particle softness and solution ionic strength [14]. In turn, Boltzmann accumulation of metal ions in the intraparticulate HNP volume and/or in the interfacial double layer region formed with the outer electrolyte solution can be estimated making use of independent electrokinetic or protolytic titration data whose interpretation provides the required density of reactive charges carried by the complexants [23–25]. Important developments of the theoretical framework include the impact of background counter-ions accumulation within the particle body during equilibration of the charged particulate complexant with its ionic atmosphere [26], and the account of Manning-like condensation of metals in the intraparticulate double layer region of highly-charged complexants [2–4,19,27]. Identification of the effective region of metal ions accumulation inside or beyond the physical volume of the complexants corrected for electric double layer extension is a further option provided by the theory [23].

So far, the above generic theoretical framework has been successfully applied to quantify the extent by which particle electric field contributes to binding of common divalent metal cations (*e.g.* Cd(II), Cu(II) or Pb(II)) to humic and fulvic nanoparticles [2,3,5]. While the underlying mechanistic aspects of divalent metal complexation are now better understood, the binding of higher-valence metals to HNP still requires detailed investigation free of the over-simplified electrostatic descriptors subsumed in NICA-Donnan or WHAM/Model VII speciation concepts. Such analysis is all the more necessary as impacts of particle electrostatics on metal complexation is expected to increase with metal valence according to an exponential manner, as anticipated from the conventional form of Boltzmann metal accumulation factor. Due to their abundance in the critical zone and the key roles played by trivalent metal ions in various microbial and geochemical processes [28] or their differentiated toxicity with respect to oxidation state [29], efforts have been undertaken to analyse the complexation of Cr(III) [30], Al(III) and Fe(III) [31] by humic substances *via* the only prism of approximate NICA-Donnan or WHAM/Model VII interpretative frameworks. Speciation of other elements like Eu(III) is also documented due to its use as an analogue for predicting transport of radionuclides in the geosphere [32]. Given the above elements, the objective of the current study is to address the intrinsic chemical binding affinity of indium to HNP in the light of latest knowledge on ionic reactivity of nanoparticles [19]. The purpose is to achieve a proper discrimination between electrostatic and chemical components of HNP-In complexes. For this work, the choice of indium as a model trivalent metal ion is further motivated by its aqueous geochemistry dominated by hydroxo-

complexes formation, very analogous to that of aluminum or rare earth metals like scandium and gallium, used for the production of semi-conducting materials [33]. In detail, indium cation binding to humic nanoparticles with radius 5 nm is addressed at various metal-to-ligand ratios as a function of background $NaClO_4$ electrolyte concentration using the equilibrium electroanalytical technique AGNES (Absence of Gradient and Nernstian Equilibrium), well-adapted to measure accurately a large range of free In(III) concentrations in solution down to the nM level [34,35]. The study was carried out at pH=4.0 where there is a significant amount of trivalent indium ions and deprotonated HNPs carboxyl groups. Interpretation of the data is supported by the independent evaluation of some relevant electrostatic descriptors of humic nanoparticles from PB-based modelling of protolytic titration measurements. Use of these descriptors within theory for ionic partition equilibration of charged nanoparticles in aqueous media [26] leads to (i) consistent estimation of the intraparticulate accumulation volume of In(III) pending proper account of indium hydroxo-complexes formation in bulk solution, and (ii) evaluation of the pristine chemical component of In(III) binding to HNP nano-complexant. Results are further discussed in relation to stability constants available for divalent and other trivalent metal-HNP complexes.

MATERIALS AND METHODS

The concentration of free indium metal species in bulk medium where HNPs were dispersed (see details below) was determined by AGNES [34,36], using a thin mercury film deposited on a rotating disk electrode as the working electrode.

Humic acid sample. Humic substance extracted from soils was separated based on their solubility properties according to three fractions: fulvic acids that are always soluble at any pH, humic acids that are insoluble in acid media, and humin that is insoluble. Humic acid nanoparticles (HNPs) used in this work were extracted following the IHSS procedure for soil organic matter [37] from peat in the Mogi river region of Ribeirão Preto, São Paulo State, Brazil. Elemental analysis (CHN) yielded C: 51.3%; H: 4.2% and N: 3.8% with an ash content of 0.6% [38]. The HNP radius (r_p) was determined by scanned stripping chronopotentiometry with $r_p = 5.0 \pm 1.4$nm [25].

Preparation of HNPs solution batches. All solutions used for the experiments were prepared with ultra-pure water (18.2 MΩ cm, Elga labwater). In(III) solutions were obtained from dilution of a 1000 mg L^{-1} certified standard solution (Fluka). The ionic strength of the HNP suspension was fixed with sodium perchlorate ($NaClO_4$) (Fluka, purity>>98%). Perchlorate acid ($HClO_4$) (Fluka) or sodium hydroxide (NaOH) (Merck suprapur) solutions were further used to adjust solution pH. Batch suspensions of 5 mg L^{-1} purified humic acids were so prepared in 10, 30 and 100 mM $NaClO_4$ electrolyte, systematically in large excess over the indium metal species whose total concentration $c^*_{In,total}$ was in the range 0.1 µM to 2.5 µM. Solution pH was adjusted to 4.00 upon addition of $HClO_4$. At this selected pH and concentration level, there is no precipitation of indium. Prepared solutions

were equilibrated at least for 24 h prior to measurements. During electroanalytical measurements, oxygen elimination in the HNP batches was performed using Nitrogen (> 99.999% pure) purchased from Air Liquide.

Electrochemical measurements. An Ecochemie Autolab type III potentiostat controlled by GPES 4.9 software (Ecochemie, The Netherlands) was used in conjunction with a Metrohm 663VA stand. Dri-ref-5 electrode from WPI (Sarasota, FL, U.S.A.) and a glassy carbon electrode were used as reference and counter electrode, respectively. The working electrode was a thin mercury film plated onto a rotating glassy carbon disk of 2 mm diameter (Metrohm) as detailed in Supporting Material (SM, section A). The rotating disk/thin mercury film electrode was renewed on a daily basis for each set of experiments. AGNES measurements were performed according to the following protocol. Metal deposition step at the mercury electrode was achieved by applying a potential E_d maintained constant during a suitable deposition time (t_d) under agitation conditions (1000 rpm rotation speed). The magnitude of the potential E_d was chosen in order to accumulate enough indium to be detected, and t_d was fixed so as to reach the situation in line with Nernstian equilibrium and absence of metal concentration gradients in the vicinity of the electrode surface [34,36,39]. Under our experimental conditions, E_d was varied from -0.570V to -0.590V *vs* Ag/AgCl and t_d in the range 120s to 160s. Regarding the stripping step, the oxidizing current was equal to 3µA. At equilibrium, the gain (or preconcentration factor) Y is the ratio between the concentration of indium amalgamated in the mercury electrode and the concentration of the oxidised metal form in solution. It has been shown that the corresponding measured accumulated charge Q_{In} is proportional to the free (hydrated cation) metal concentration, which reads for indium:

$$Q_{In} = Y\,\eta_Q\,c^*_{\mathrm{In}^{3+}} \quad (1)$$

where $c^*_{\mathrm{In}^{3+}}$ is the free indium concentration in bulk solution and η_Q is the proportionality factor

$$\eta_Q = 3\,F\,V_{Hg} \quad (2)$$

where F is the Faraday constant and V_{Hg} is the volume of the mercury electrode. A disposable polystyrene cell was placed in a double-walled container connected to a refrigerating-heating circulator and the temperature of the tested solution was set to 25°C. The solution was initially purged with nitrogen for 15 min, and afterwards a nitrogen blanket was systematically maintained above the sample solution. Prior to determination of $c^*_{\mathrm{In}^{3+}}$ in the HNPs solution batches, a calibration plot was performed using the AGNES parameters (E_d; t_d) previously mentioned. Calibration measurements consists in preparing a 20 mL solution with composition: 10, 30 or 100 mM $NaClO_4$, 60 µL of 1M $HClO_4$ to fix the pH at 2.5, so that ca. 95% of indium is in free form. This value is estimated regarding the stability constants of the first and second indium hydroxide species derived from the stripping chronopotentiometry data recently reported in Galceran *et al.*,[35] with $\log\beta_1$=-3.37 and $\log\beta_2$=-6.95 at infinite dilution. More details on the evaluation of $\log\beta_1$ and $\log\beta_2$ are provided in SM (section B). Then, several additions of 10 µM and 100 µM indium stock solution were performed to construct the

calibration curve. After this procedure, the equilibrated batch solution containing HNPs with the lowest total indium concentration was disposed in the electrochemical cell and AGNES measurements were repeated three times. Upon appropriate addition of concentrated indium solution (10 µM or 100 µM), several total concentrations of indium were tested. The same protocol was iterated with a second batch having a higher total indium concentration. Under the pH condition of interest in this work (pH=4.0), the free indium ions are in equilibrium with hydroxide species, mainly $In(OH)^{2+}$ and $In(OH)_2^+$ (see SM, section B for further details). Starting from the free ion concentrations determined experimentally, bulk $In(OH)^{2+}$ and $In(OH)_2^+$ concentrations, $c^*_{In(OH)^{2+}}$ and $c^*_{In(OH)_2^+}$, respectively, were computed using Visual MINTEQ software [40]. The smeared-out concentration $\bar{c}_{In,b}$ of all forms of indium associated with HNPs in the whole sample volume was then directly obtained from the mass balance equation involving the relevant indium metal species, *i.e.* $\bar{c}_{In,b} = c^*_{In,\,total} - c^*_{In^{3+}} - c^*_{In(OH)^{2+}} - c^*_{In(OH)_2^+}$.

THEORY

Boltzmann accumulation factors of Indium at HNPs.

Following previous work on the binding of divalent metals to nanoparticulate fulvics [5], the Boltzmann factors pertaining to the partitioning of the cationic indium species between HNP body and bulk solution were estimated on the basis of the potential profile operational within and outside charged HNPs and determined *with or without accounting* for the neutralization of the structural HNP charges following intra- and extra-particulate accumulation of counterions from electrolyte solution. In both situations considered, the evaluation of the potential profile calls for solving the nonlinear Poisson Boltzmann (PB) equation [41] along the lines we detailed elsewhere [26]. This evaluation requires knowledge of the particle radius (r_p) and the volume density of pristine structural charges carried by HNPs ($\rho_0^{(s)}$) under the relevant pH and salt concentration conditions [25] (see 'Electrostatic and protolytic descriptors of HNPs' in Results and discussion, for the evaluation of $\rho_0^{(s)}$ of our HNPs system). r_p was estimated from scanned stripping chronopotentiometry, leading to r_p = 5.0±1.4nm [25], and $\rho_0^{(s)}$ from our recent interpretation of HNPs protolytic titration data *vs* pH and salt concentration using Soft Poisson Boltzmann-based Titration formalism for nanoparticles (SPBT) [25]. We briefly recall below how the relevant Boltzmann accumulation factors of indium species inside and in the vicinity of charged HNPs is formulated for the two envisaged scenarios.

Boltzmann accumulation of indium metal species without account of HNPs charge neutralization by intra/extra particulate counterion accumulation.

The electrostatic potential distribution across the HNPs is denoted as $y^{(s)}(r)$ where r is the radial coordinate with the origin r=0 set at the particle center. $y^{(s)}(r)$ was evaluated by numerical solving of

the nonlinear Poisson-Boltzmann differential equation established for permeable nanoparticles defined by given r_p and $\rho_0^{(s)}$ and dispersed in 1:1 $NaClO_4$ electrolyte [26,41]. The resulting Boltzmann factor $\bar{f}^{(s)}_{B,In^{3+}}$ of *e.g.* In^{3+} ions accumulated from *r*=0 to *r*=*R* with *R* the radius of the accumulation volume, is then simply given by:

$$\bar{f}^{(s)}_{B,In^{3+}} = 3R^{-3}\int_0^R r^2 \exp\left[-3y^{(s)}(r)\right]dr\,, \tag{3a}$$

and the Boltzmann factors $\bar{f}^{(s)}_{B,In(OH)^{2+}}$, $\bar{f}^{(s)}_{B,In(OH)_2^+}$ for $In(OH)^{2+}$ and $In(OH)_2^+$ are provided by:

$$\bar{f}^{(s)}_{B,In(OH)^{2+}} = 3R^{-3}\int_0^R r^2 \exp\left[-2y^{(s)}(r)\right]dr \tag{4b}$$

$$\bar{f}^{(s)}_{B,In(OH)_2^+} = 3R^{-3}\int_0^R r^2 \exp\left[-y^{(s)}(r)\right]dr \tag{5c}$$

The overall Boltzmann accumulation factor $\bar{f}^{(s)}_{B,In}$ for the ensemble of indium species then directly follows Eq. (3) after proper ponderation of the bulk concentration of each indium species, *i.e.*

$$\bar{f}^{(s)}_{B,In} = \frac{\bar{f}^{(s)}_{B,In^{3+}} \times c^*_{In^{3+}} + \bar{f}^{(s)}_{B,In(OH)^{2+}} \times c^*_{In(OH)^{2+}} + \bar{f}^{(s)}_{B,In(OH)_2^+} \times c^*_{In(OH)_2^+}}{c^*_{In}}\,. \tag{4}$$

Boltzmann accumulation of indium metal species accounting for effects connected to the accumulation of counterions from background electrolyte.

In this second situation, the impact of counterion accumulation at/within the particle body/surface during equilibration of HNP with its ionic atmosphere is accounted for. Such counterion accumulation effectively lowers the magnitude of the net HNP charge density, which may significantly affect the extent to which indium species are electrostatically associated to HNPs, and it thus may impact on their respective Boltzmann partitioning coefficient. The theoretical framework was reported by Duval *et al.*[26] and it is based on an iterative procedure for finding the equilibrated situation defined by the relationship $Q^{0,eq} = -\rho_0^{(eq)} V_p$, where $Q^{0,eq}$ is the total amount of charges originating from counterions accumulated within and/or outside the charged HNP body of volume V_p, and $\rho_0^{(eq)}$ corresponds to the resulting net density of HNP structural charges. Once $\rho_0^{(eq)}$ is obtained, the associated $y^{(eq)}(r)$ directly follows from the PB equation, and the equilibrated concentration $c_X^{(eq)}$ of the metal species X distributed in the accumulation sphere of radius *R* can be computed following the method detailed in Town *et al.*[5] for divalent metals after straightforward adaptation to the case of mono-, di- and tri-valent indium species and 1:1 background electrolyte (of interest in this work). The accumulation Boltzmann factor pertaining to each indium species is then simply given by:

$$\bar{f}^{(eq)}_{B,In^{3+}} = c^{(eq)}_{In^{3+}} / c^*_{In^{3+}}\,, \tag{5a}$$

$$\bar{f}^{(\mathrm{eq})}_{\mathrm{B,In(OH)^{2+}}} = c^{(\mathrm{eq})}_{\mathrm{In(OH)^{2+}}}/c^{*}_{\mathrm{In(OH)^{2+}}} \quad (5b)$$

$$\bar{f}^{(\mathrm{eq})}_{\mathrm{B,In(OH)_2^{+}}} = c^{(\mathrm{eq})}_{\mathrm{In(OH)_2^{+}}}/c^{*}_{\mathrm{In(OH)_2^{+}}}, \quad (5c)$$

and the total Boltzmann factor $\bar{f}^{(\mathrm{eq})}_{\mathrm{B,In}}$ for the ensemble of indium metal species is now given by :

$$\bar{f}^{(\mathrm{eq})}_{\mathrm{B,In}} = \frac{\bar{f}^{(\mathrm{eq})}_{\mathrm{B,In^{3+}}} \times c^{*}_{\mathrm{In^{3+}}} + \bar{f}^{(\mathrm{eq})}_{\mathrm{B,In(OH)^{2+}}} \times c^{*}_{\mathrm{In(OH)^{2+}}} + \bar{f}^{(\mathrm{eq})}_{\mathrm{B,In(OH)_2^{+}}} \times c^{*}_{\mathrm{In(OH)_2^{+}}}}{c^{*}_{\mathrm{In}}}. \quad (6)$$

For the sake of conciseness, we refer below to either equilibrated (eq) or structural (s) -with a common superscript (eq,s)- to embrace both approaches where HNP charge neutralization by counterion accumulation is accounted for or not, respectively. We stress that the contribution of indium species in the neutralization of HNP charges is insignificant *as compared to* that of counterions from background electrolyte (present in large excess over the metal species), a point that we verified upon determination of $y^{(\mathrm{eq})}(r)$ from PB equation formulated with and without including the contribution of the indium species to the overall density of mobile ionic charges at position *r*. Last, it is emphasized that the concentrations $c^{*}_{\mathrm{In^{3+}}}$, $c^{*}_{\mathrm{In(OH)^{2+}}}$, $c^{*}_{\mathrm{In(OH)_2^{+}}}$ involved in Eqs 4 and 6 are all determined experimentally, and that the evaluation of $\bar{f}^{(\mathrm{s,eq})}_{\mathrm{B,In^{3+}}}$, $\bar{f}^{(\mathrm{s,eq})}_{\mathrm{B,In(OH)^{2+}}}$ and $\bar{f}^{(\mathrm{s,eq})}_{\mathrm{B,In(OH)_2^{+}}}$ was carried out with full account of the HNP protolytic descriptors relevant under the here tested pH and salt concentration conditions. Related to the latter point, we recall that the pristine density $\rho_0^{(s)}$ of structural HNP charges required for the analysis directly follows from protolytic titration data relevant for the HNP material adopted in this work (see Results and Discussion) [25]. For given measured concentrations $c^{*}_{\mathrm{In^{3+}}}$, $c^{*}_{\mathrm{In(OH)^{2+}}}$, $c^{*}_{\mathrm{In(OH)_2^{+}}}$ and Boltzmann factors $\bar{f}^{(\mathrm{s,eq})}_{\mathrm{B,In^{3+}}}$, $\bar{f}^{(\mathrm{s,eq})}_{\mathrm{B,In(OH)^{2+}}}$ and $\bar{f}^{(\mathrm{s,eq})}_{\mathrm{B,In(OH)_2^{+}}}$ computed at given *R*, the resulting apparent stability of In-HNP complex species (with both chemical and electrostatic contributions included) can be estimated as a function of background electrolyte concentration and subsequently compared to that determined on the basis of the measured concentrations $\bar{c}_{\mathrm{In,b}}$ and c^{*}_{In}. Results are discussed in the next section. The FORTRAN computational codes developed for evaluation of $\bar{f}^{(\mathrm{s,eq})}_{\mathrm{B,In}}$ are available upon request.

RESULTS AND DISCUSSION

Electrostatic and protolytic descriptors of HNPs

The parameters describing the binding of protons to our HNP were previously obtained from analysis of protolytic titration curves according SPBT formalism [25]. The analysis provides the total charge Q^0 distributed throughout the whole HNP volume (V_p) as a function of pH and solution ionic strength. It reveals that carboxylic groups are 3 times more abundant than phenolic ones with corresponding equivalent densities of monovalent charges of -298±2 mol m^{-3} and -101±5 mol m^{-3} (expressed per

HNP volume), respectively. In addition, the analysis allowed the determination of the Langmuir-Freundlich equation parameters namely the pK_a values, centered at 4.26 ± 0.02 and 8.57 ± 0.09 and the distribution widths $m_{H,1}$ = 0.46 ± 0.01 and $m_{H,2}$ = 0.59 ± 0.03 for carboxylic (1) and phenolic (2) groups, respectively. These different HNP protolytic properties were explicitly included in the structural charge density term of the PB equation solved here to evaluate the Boltzmann accumulation factors of indium species at HNPs (see section Theory) along the lines given in Pinheiro *et al.*[25].

Electrostatic contribution to indium binding to Humic nanoparticles

Figure 1 displays the apparent stability constants $\overline{K}_{app}$ measured for indium-HNP complexes, adopting for $\overline{K}_{app}$ the definition by Town *et al.*[5], *i.e.*:

$$\overline{K}_{app} = \bar{c}_{In,b}/(c^*_{In}\times(\bar{c}_{S,t} - \bar{c}_{In,b})) \quad (7)$$

where $\bar{c}_{In,b}$ is the (measured) smeared-out concentration of all forms of indium hydroxy species associated with HNP particles over the whole sample volume, c^*_{In} is the total concentration of dissolved indium species, which includes free indium ions and hydrolysis complexes, and $\bar{c}_{S,t}$ refers to the concentration of deprotonated HNP reactive sites smeared-out over the solution volume ($\bar{c}_{S,t}$ is derived directly from the densities of charges (-298±2 mol m^{-3}), from pK_{a1} and $m_{H,1}$ values, with the end result $\bar{c}_{S,t}$=8.8 mmol m^{-3} at pH=4 [25]). Analysis of indium speciation in bulk solution showed that the trivalent indium species are still significantly present at pH 4, and in 100 mM electrolyte concentration the respective fractions of indium species read as 27%, 41% and 32% for In^{3+}, $In(OH)^{2+}$ and $In(OH)_2^+$, respectively. In **Figure 1**, $\overline{K}_{app}$ is plotted against the degree of metal occupation of HNP binding sites (*i.e.* the ratio $\bar{c}_{In,b}/\bar{c}_{S,t}$) at three $NaClO_4$ concentrations (10 mM, 30 mM and 100 mM). The measured $\overline{K}_{app}$ involves the (chemical) inner-sphere complexation of indium species with HNP reactive sites, with an intrinsic stability constant that we denote as $\overline{K}_{int}$, and an electrostatic Boltzmann factor $\bar{f}^{(exp)}_{B,In}$ ('exp' for experimental, not to confuse with the theoretical factors $\bar{f}^{(s,eq)}_{B,In}$ introduced in the preceding section), so that $\overline{K}_{app} = \bar{f}^{(exp)}_{B,In}\overline{K}_{int}$. As typical for heterogeneous complexants, $\overline{K}_{int}$ (and therewith $\overline{K}_{app}$) for HNPs depends on the metal-to-HNPs reactive sites coverage, that is, the extent to which the reactive sites are involved in inner-sphere complexation depending on their molecular environment and respective metal binding constants. For many types of humic substances, log $\overline{K}_{app}$ *vs.* log $\bar{c}_{In,b}/\bar{c}_{S,t}$ is a straight line with slope equal to $-1/\Gamma$, where Γ is the heterogeneity parameter ($0 < \Gamma \leq 1$ and $\Gamma = 1$ for the homogeneous case) [5]. As the electrolyte concentration decreases, screening of HNP charges becomes less significant, and the magnitude of both $\bar{f}^{(exp)}_{B,In}$ and $\overline{K}_{app}$ increases, in line with **Figure 1** and standard polyelectrolyte effect. This latter effect predominates over the decrease in the concentration of reactive sites (or charges) of HNP with decreasing electrolyte concentration [25]. The reason is that, regardless of the electrolyte concentration adopted here, the (charged) HNP reactive

sites are always in large excess over the indium metal species. At fixed $\bar{c}_{\mathrm{In,b}}/\bar{c}_{\mathrm{S,t}}$, the increase in $\overline{K}_{\mathrm{app}}$ with decreasing electrolyte concentration thus directly reflects the way electrostatics affects indium complexation by HNP. We observe that the difference between two sets of $\overline{K}_{\mathrm{app}}$ data collected under different salinity conditions is constant over the whole range of metal-to-HNP load (or $\bar{c}_{\mathrm{In,b}}/\bar{c}_{\mathrm{S,t}}$) studied here. This finding supports that the contribution of electrostatics on In-HNP complex stability is independent of the range of metal-to-HNP reactive sites coverage explored in this study. In other words, the particulate electric field is not affected by the neutralization of negative HNP charges by metal ions, which agrees with conclusion based on the (similar) solution to PB equation obtained with or without including HNP charge neutralization by indium species (counterions from $NaClO_4$ are always in large excess over indium).

The experimental Boltzmann factor $\bar{f}_{\mathrm{B,In}}^{(\mathrm{exp})}$ can be derived following the strategy detailed by Town *et al.*[5] provided that $\overline{K}_{\mathrm{app}}$ values can be measured at electrolyte concentrations sufficiently high for the HNP charge screening to be so significant that $\bar{f}_{\mathrm{B,In}}^{(\mathrm{exp})} \to 1$ (case where electrostatic contribution to metal binding is insignificant). Exploiting such a 'reference situation', $\bar{f}_{\mathrm{B,In}}^{(\mathrm{exp})}$ operative at a given salt concentration can then be directly quantified from the ratio between slopes of the curve $\overline{K}_{\mathrm{app}}$ *vs.* $\bar{c}_{\mathrm{In,b}}/\bar{c}_{\mathrm{S,t}}$ (plotted in double logarithmic representation) evaluated at the tested salinity and at that corresponding to the aforementioned 'reference situation' [5]. In this work, we checked that the experimental identification of this 'reference situation' is not possible due to the aggregation of HNPs occurring at salt concentrations ≥ 150mM. Accordingly, to circumvent this difficulty and proceed to data analysis and confrontation with theoretical predictions, we evaluate below the electrostatic contributions to In complexation by HNPs at $c_{\mathrm{elec}}^{\infty} = 10$ and 30 mM relative to that at 100 mM, where $c_{\mathrm{elec}}^{\infty}$ refers to bulk concentration of $NaClO_4$. These relative electrostatic contributions to metal binding correspond to the ratios $\bar{f}_{\mathrm{B,In,10mM}}^{(\mathrm{exp})}/\bar{f}_{\mathrm{B,In,100mM}}^{(\mathrm{exp})}$ or $\bar{f}_{\mathrm{B,In,30mM}}^{(\mathrm{exp})}/\bar{f}_{\mathrm{B,In,100mM}}^{(\mathrm{exp})}$, *i.e.* to the slope of the log-log plots $\overline{K}_{\mathrm{app}}$ *vs.* $\bar{c}_{\mathrm{In,b}}/\bar{c}_{\mathrm{S,t}}$ estimated at 10mM and 30 mM divided by that at 100mM, respectively.

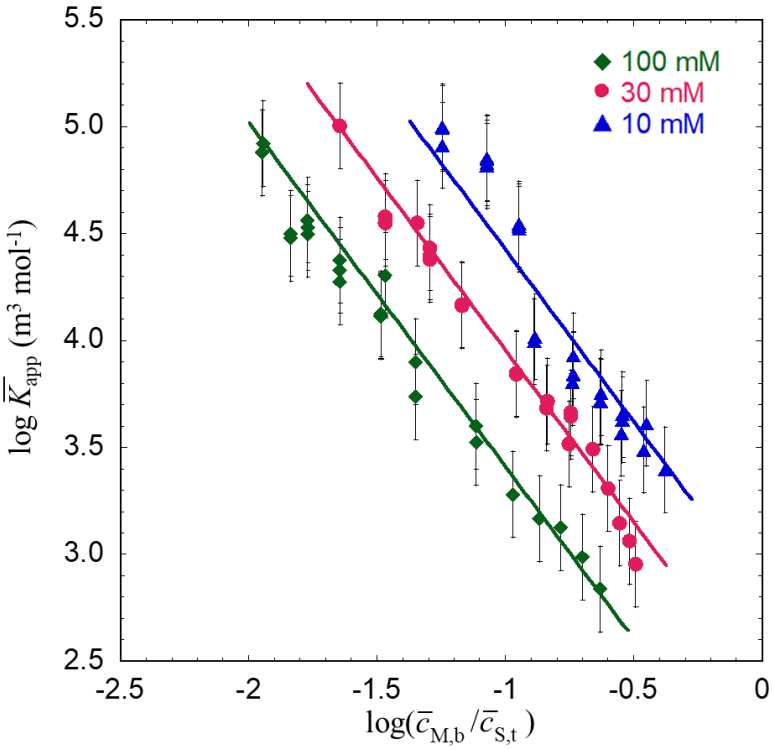

Figure 1: Apparent stability constants $\overline{K}_{app}$ for the indium complexes formed with nanoparticulate humics as a function of the degree of association of In with HNP reactive sites, measured at c^{∞}_{elec} = 10mM, 30mM, 100mM $NaClO_4$ concentration and pH=4. Lines correspond to linear regression of experimental data with slopes equal to -1.61 for the three ionic strengths. Error bars refer to calculation uncertainties of $\overline{K}_{app}$ estimated from the experimental errors on the indium concentration measurements.

Figure 2 reports the ratios $\bar{f}^{(exp)}_{B,In,10mM}/\bar{f}^{(exp)}_{B,In,100mM}$ and $\bar{f}^{(exp)}_{B,In,30mM}/\bar{f}^{(exp)}_{B,In,100mM}$ together with those estimated from theory, *i.e.* $\bar{f}^{(s,eq)}_{B,In,10mM}/\bar{f}^{(s,eq)}_{B,In,100mM}$ and $\bar{f}^{(s,eq)}_{B,In,30mM}/\bar{f}^{(s,eq)}_{B,In,100mM}$ that pertain to the situations where structural (s) or equilibrated (eq) HNPs charge densities are considered to estimate the Boltzmann partitioning coefficients of In (see section Theory). Theoretical computations are provided as a function of the radius *R* of the metal accumulation sphere, with *R* being the *only* parameter adjusted to reach consistent fitting of the experimental data at the different solution ionic strength conditions tested in this work.

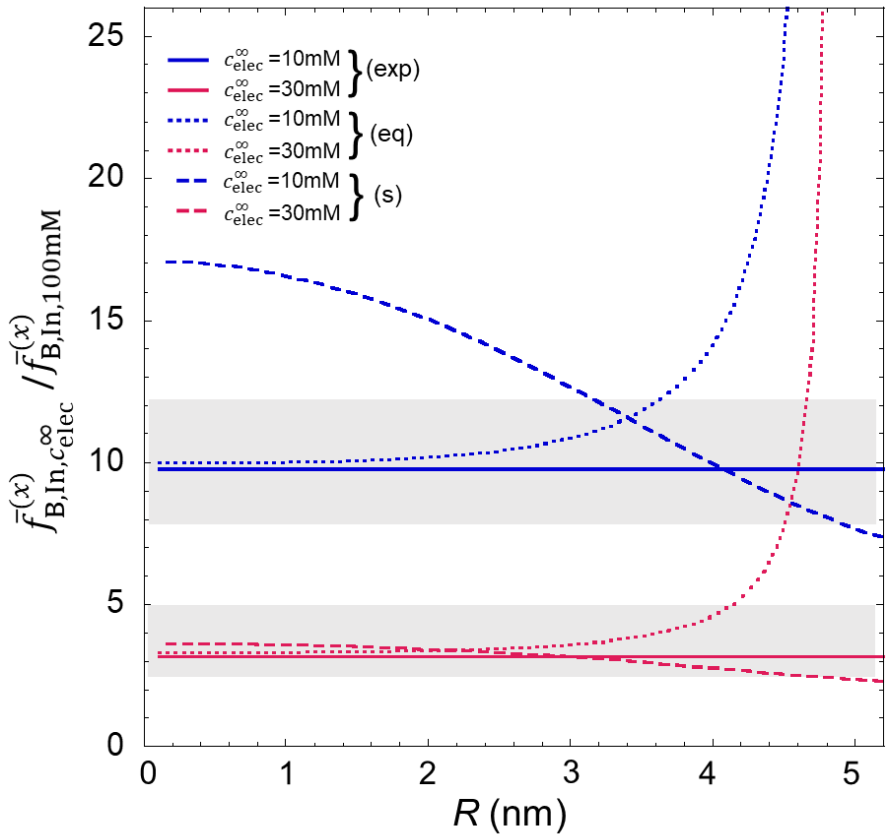

Figure 2: Comparison between electrostatic Boltzmann partitioning coefficients of In at HNP/solution interface as derived from experiments and theory ($\bar{f}^{(x)}_{B,In,c^{\infty}_{elec}} / \bar{f}^{(x)}_{B,In,100mM}$) as a function of R, the radius of the accumulation volume. The superscript (x) specifies how the $\bar{f}_{B,In}$-ratios were derived, with $(x)\equiv$(exp) for factors derived from experiments, and $(x)\equiv$(s) and $(x)\equiv$(eq) for ratios estimated from theory considering structural (s) or equilibrated (eq) HNP charge density, respectively. See text for details. c^{∞}_{elec} refers to the background $NaClO_4$ electrolyte concentration (10, 30 mM and 100 mM). The grey domains capture the limits of the $\bar{f}^{(exp)}_{B,In}$ ratios estimated from linear regressions of the $\bar{K}_{app}$ *vs.* $\bar{c}_{M,b}/\bar{c}_{S,t}$ log-log plots with including their dispersion reflected by the errors bars in Figure 1.

Figure 2 shows a good agreement between experiments and theory based on the structural (s) HNP charge density for computation of the electrostatic potential distribution. Within experimental uncertainties, $\bar{f}^{(s)}_{B,In,30mM}/\bar{f}^{(s)}_{B,In,100mM}$ is identical to $\bar{f}^{(exp)}_{B,In,30mM}/\bar{f}^{(exp)}_{B,In,100mM}$ for $0<R\sim5$ nm, whereas $\bar{f}^{(s)}_{B,In,10mM}/\bar{f}^{(s)}_{B,In,\ 100mM}$ compares well to measured data for $\sim3.5<R\sim5$ nm. Closer inspection of the data reveals that $\bar{f}^{(s)}_{B,In,10mM}/\bar{f}^{(s)}_{B,In,\ 100mM}$ significantly overestimates $\bar{f}^{(exp)}_{B,In,10mM}/\bar{f}^{(exp)}_{B,In,\ 100mM}$ for decreasing values of R. This trend simply reflects the neglect of the decrease in HNP charge density as a result of HNP charge neutralization by counterion accumulation in the intraparticulate HNP body. The lower is the electrolyte concentration, the most significant becomes the effect of HNP charge neutralization on the particle electric field. All in all, results at 10 mM and 30 mM treated on the basis of the structural (s) HNP charge density within PB formalism are in line with an accumulation of indium cations that spans over the intraparticulate volume. This finding for indium contrasts with the conclusions obtained

for the binding of divalent metal cations (Cd(II), Cu(II)) to highly charged nanoparticulate fulvics [5]. For the latter particles with size of the order of the Debye layer thickness ($1/\kappa$) under practical salinity conditions (as it is the case for the HNPs considered here, with κr_p ~1.67 and κr_p~0.5 at c_{elec}^{∞} =10 mM and 100 mM, respectively), a significant accumulation of the metals proceeds in an extraparticulate (condensation) zone, which points to the involvement of counterion condensation phenomena as examined by Manning for linear polyelectrolytes. This difference likely originates from the charge density of the fulvics in Town *et al.*[5] that is ca. five times larger than that of our HNPs. Such high charge density of the fulvics advocates for the occurrence of Manning-like condensation of metal ions.

The agreement between theoretical and experimental Boltzmann factors is greatly enhanced pending account of HNP charges neutralization by electrolyte counterions. Indeed, the Boltzmann factor ratios derived from experiments at 10 mM and 30 mM remarkably match the ratios $\bar{f}_{B,In,10mM}^{(eq)}/\bar{f}_{B,In,100mM}^{(eq)}$ and $\bar{f}_{B,In,30mM}^{(eq)}/\bar{f}_{B,In,100mM}^{(eq)}$ for values of *R* in the range 0<*R*~3.5 nm at both 10 mM and 30 mM $NaClO_4$. In line with results given for divalent metals [5], this finding confirms that equilibrated ion partitioning provides the best description for the electrostatic contribution to metal complexation by charged nanoparticles as a function of electrolyte concentration.

We now report in **Figure 3** the electrostatic potential profiles $y(r)^{(s)}$ and $y(r)^{(eq)}$ evaluated from PB equation that integrates either equilibrated or structural HNP charge density. Both $y(r)^{(s)}$ and $y(r)^{(eq)}$ profiles show a bell-shaped form, thus confirming that the commonly adopted Donnan electrostatic model [16,42] is not relevant for nanoparticles in the thick double layer regime where κr_p~1. When discarding HNP charge neutralization by counterions, the corresponding electrostatic potential profile in the particle body is significantly overestimated compared to that computed with integrating HNP charge equilibration with its counterion atmosphere. **Figure 3** further shows that in the innermost part of HNPs, the order (with varying electrolyte concentration) of the equilibrated electrostatic potential profile is reversed compared to that obtained with considering the structural charge density of HNPs within PB equation, in agreement with Duval *et al.*[26]. In the latter case, the potential (in absolute value) decreases at fixed position with increasing electrolyte concentration due to conventional particle charge screening.

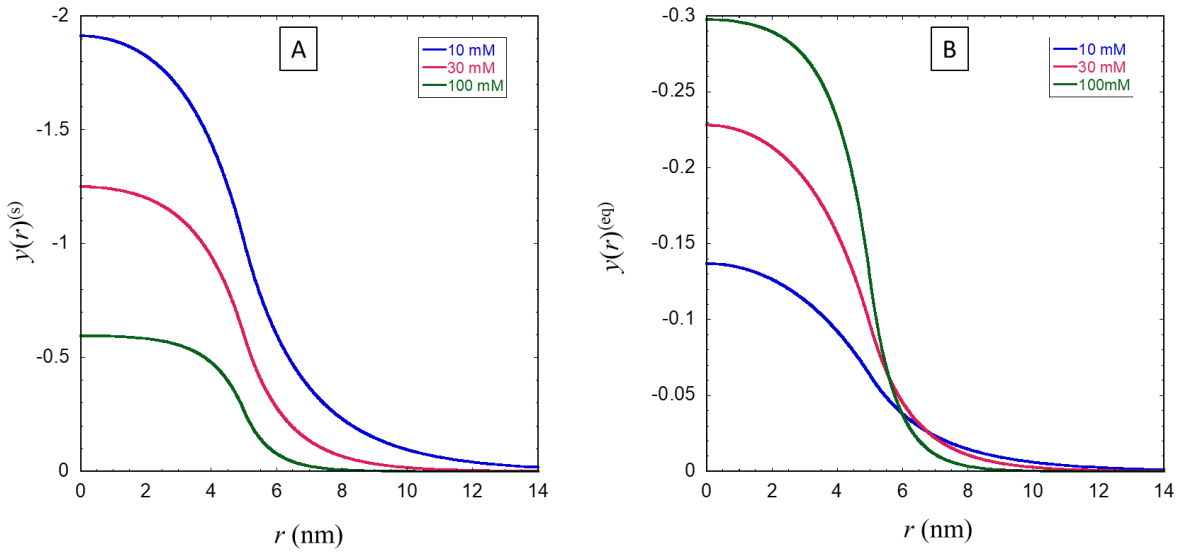

Figure 3 : Electrostatic potential profiles obtained from PB equation using the structural (A) and equilibrated (B) HNP charge density for c^{∞}_{elec}=10mM, 30mM, 100mM (specified). In (B), computations were carried out with a counterion accumulation volume of radius R=4nm.

The ratios $\bar{f}^{(\text{eq})}_{\text{B,In},c^{\infty}_{\text{elec}}}/\bar{f}^{(\text{eq})}_{\text{B,In, 100mM}}$ are found nearly constant for radius R of metal accumulation volume lower than ca. 3 nm (**Figure 2**), which basically corresponds to the intraparticulate region where the dependence of $y(r)^{(\text{eq})}$ on r is weakest and potential largest in magnitude (**Figure 3**). Unlike $\bar{f}^{(\text{s})}_{\text{B,In},c^{\infty}_{\text{elec}}}/\bar{f}^{(\text{s})}_{\text{B,In, 100mM}}$, $\bar{f}^{(\text{eq})}_{\text{B,In},c^{\infty}_{\text{elec}}}/\bar{f}^{(\text{eq})}_{\text{B,In, 100mM}}$ increases dramatically for $R \sim r_{\text{p}}$, and this behavior corresponds to the limit $\rho_{\text{o}}^{(\text{eq})} / \rho_{\text{o}}^{(\text{s})} \to 1$ where it is impossible to accommodate more counterions within the electric double layer in order to compensate for NP structural charges [26].

Now that the electrostatic contribution to In-HNP association has been evaluated, in the next section we discuss the intrinsic chemical component $\bar{K}_{\text{int}}$ of the apparent stability constant $\bar{K}_{\text{app}}$ of In-HNP complexes.

Intrinsic stability constants for indium-HNP complexes

The intrinsic stability constant $\bar{K}_{\text{int}}$ of In-HNP complexes is defined by [5]:

$$\bar{K}_{\text{int}} = \frac{c_{\text{InS}}}{c_{\text{S}} c_{\text{In}}} \qquad (8)$$

where c_{InS}, c_{S} and c_{In} are the local intraparticulate concentrations of In-HNP inner-sphere complexes, the concentration of unoccupied reactive sites within the particle and the concentration of unbound indium species in HNP body, which encompasses both free indium cations and hydrolysis products, respectively. c_{In} follows directly from c^{*}_{In} and c_{InS} according to:

$$c_{\mathrm{InS}} = \frac{c^{*}_{\mathrm{In,total}} - c^{*}_{\mathrm{In}}}{\varphi} - c_{\mathrm{In}} \quad (9)$$

where $c^{*}_{\mathrm{In,total}}$ is the total indium concentration in solution, c^{*}_{In} is the bulk solution concentration of the dissolved indium species, and φ stands for the HNP volume fraction estimated from the product between the HNP mass concentration (5 10^{-3} kg m^{-3}) and the HNP specific hydration volume (0.0137 m^3 kg^{-1}) [25].

Estimation of c_{In} is done by using the equation :

$$c_{\mathrm{In}} = \bar{f}^{(\mathrm{eq})}_{\mathrm{B,In}} \times c^{*}_{\mathrm{In}} \quad (10)$$

where we adopted the Boltzmann accumulation factor evaluated from equilibrated HNP charge density because this strategy consistently describes the experimental results at both 10 and 30 mM $NaClO_4$ concentration with $R \leq$ 3.5nm (**Figure 2**). Accordingly, values of $\overline{K}_{\mathrm{int}}$ obtained from Eqs 8-10 are reported in **Figure 4** as a function of the coverage degree θ_{M} being the ratio between the concentrations of the inner-sphere indium complexes and the total reactive sites ($\theta_{\mathrm{M}} = c_{\mathrm{InS}}/c_{\mathrm{S,t}}$) and for various accumulation radii R satisfying $R \leq$ 3.5nm. Analysis reveals that all data collected at 10 mM, 30 mM and 100 mM $NaClO_4$ concentrations fall within a single master curve where $\log \overline{K}_{\mathrm{int}}$ decreases linearly with $\log \theta_{\mathrm{M}}$. This linearity is best preserved for R=2.5 nm as judged from analysis of the linear regression at various values of R in line with $R \leq$ 3.5nm. The correctness and consistency of our identification of the electrostatic component of indium binding to HNP are evidenced by the merging of all $\overline{K}_{\mathrm{int}}$ values within a master curve where $\overline{K}_{\mathrm{int}}$ were estimated from $\overline{K}_{\mathrm{app}}$ collected at different electrolyte concentrations (**Figure 1**). **Figure 4** thus reports the intrinsic chemical contribution $\overline{K}_{\mathrm{int}}$ to the stability of In-HNP complexes after proper correction of the data given in **Figure 1** for electrostatic effects.

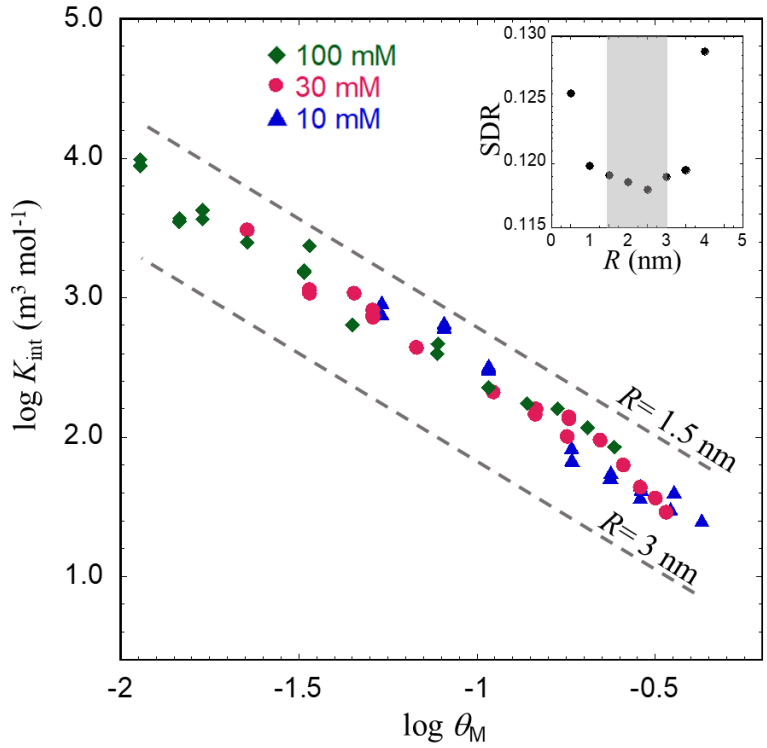

Figure 4: Intrinsic (chemical) stability constant $\overline{K}_{int}$ of indium-HNP complexes at pH=4.00 as a function of the degree of association of In with HNP reactive sites, namely the coverage degree θ_M at different radii R (indicated) for the sphere of metal accumulation within HNP. Points are calculated for R=2.5nm, with green, red and blue points corresponding to data at 100 mM, 30mM, 10mM ionic strength, respectively. Dashed lines represent linear regressions of derived log $\overline{K}_{int}$ *vs.* log θ_M plot for R=3 and 1.5 nm. The inset displays the dependence of the standard deviation of the residuals (SDR) associated with linear regressions of log $\overline{K}_{int}$ *vs.* log θ_M plot on the radius R, and the grey zone in the inset depicts the range of R values where SDR is less than 1% of the minimum SDR value obtained for R=2.5 nm.

For an accumulation radius R=2.5 nm, we find an $\bar{f}_{B,In}^{(eq)}$ that equates 12, 40 and 120 at 100mM, 30mM and 10mM $NaClO_4$ electrolyte concentration, respectively. For the sake of comparison, values of $\bar{f}_{B,Cd}^{(eq)}$ pertaining to binding of Cd(II) to highly-charged fulvics were found to be in the range 3 to 10 and 12 to 57 in 100 mM and 10 mM KNO_3 electrolyte, respectively [5]. Then, even for HNPs systems featuring a charge density that is much lower than that for the nanoparticulate fulvics examined in Town *et al.*[5], the binding of multivalent indium species to HNPs remains dramatically impacted by electrostatics. This reveals the major effect of the valence of the metal ions on their interaction with organic matter even if the latter is poorly to moderately charged.

Now that we have defined the intrinsic stability constant $\overline{K}_{int}$ of In-HNP complexes, the heterogeneity parameter Γ invoked while commenting **Figure 1** can be safely estimated from the slope of the double logarithmic representation $\overline{K}_{int}$ *vs.* θ_M (**Figure 4**) according to the Freundlich-type equation *i.e.* logθ_M = constant - Γ log$\overline{K}_{int}$, with the result Γ=0.64. This value denotes a moderate heterogeneous

binding of indium by HNP reactive sites, very similar to that of Cd(II) by highly charged humics ($\bar{\Gamma}$=0.6) [5], but significantly less heterogeneous than the complexation of Cu(II) by humics ($\bar{\Gamma}$=0.2) at pH=6 [5]. The latter difference possibly originates from our low pH (pH=4) where only a modest fraction of the carboxylic groups is involved in the indium binding process, contrary to higher pH (*e.g.* pH=6) where binding proceeds over a larger fraction of carboxylic sites and possibly phenolic sites.

Even at pH=4, **Figure 4** evidences a range of relatively high log $\bar{K}_{int}$ (m^3 mol^{-1}) values (between 4.0 to 1.5) achieved at low (log -2 or 1%) to moderate metal-to-reactive sites coverage (log -0.3 or 50%). For the sake of comparison, Town *et al.*[5] determined at pH=6 log $\bar{K}_{int}$ for Cd(II) complexation by humics with values from 0.25 to -2.5 and coverage degrees from 0.3 to 10%, thus denoting smaller complexation than that evidenced here for indium. The log $\bar{K}_{int}$ for Cu(II) complexation by humics reported in[5] ranges from 6 to -2 from 0.3 to 30% coverage degree, *i.e.* a stronger complexation than indium at low coverage, probably connected to the larger heterogeneity ($\bar{\Gamma}$=0.2). At higher coverage (above 50 %), indium complexation becomes stronger than copper probably due to the higher intrinsic affinity of the carboxylic sites for trivalent as compared with divalent metal ions [43], generally observed for rare earth elements like actinides or lanthanides as a result of multidentate binding with carboxylic groups [44,45]. A stronger binding of trivalent metal cations compared to that of divalent ones is also observed from complexation data analysed with help of the generic NICA parameters for metal ion complexation by humic matter [16], with reported log complexation constant values of 6.0 for Fe(III)-fulvics complexation, 3.5 for Fe(III)-humics, 2.8 for Cr(III)-fulvics and 4.3 for Cr(III)-humics, which are generally two to three orders magnitude higher than those reported for divalent cations.

Following this qualitative comparison with results derived from standard NICA model where Donnan electrostatics is considered, we attempted to interpret quantitatively the complexation data reported in **Figure 1** for indium-humics as a function of metal-to-reactive site coverage and electrolyte concentration making using of the NICA-Donnan (NICAD) model. More details of the NICA-Donnan approach and the fitting procedures are given in the section C of the SM. For that purpose and to avoid any bias in the comparison with results obtained on the basis of advanced Poisson Boltzmann-based modeling, we adopted here the protolytic properties of our HNP materials as derived from the NICA-Donnan modeling of HNP titration curves reported by Botero *et al.*[38] who worked on the same HNP system as that adopted here. Accordingly, attempts to reconstruct the data in **Figure 1** with NICA-Donnan model were performed making use of the parameters describing the protolytic features of the carboxylic sites (sites 1), the only relevant at pH=4 where indium complexation experiments were carried out. Site densities (Q_{max1}), protolytic parameters ($\bar{K}_{H,1}$, $m_{H,1}$ being equal $n_{H,1} \times p_1$ (see the NICA equation S9 in SM)) and HNP heterogeneity parameters (p_1) implemented for data reconstruction with NICA-Donnan model were therefore $Q_{max,1}$ =3.18 ± 0.92 mol per kg of HNP, log $\bar{K}_{H1}$=3.65 ± 0.23, $m_{H,1}$ =0.66, $n_{H,1}$=0.84±0.04 and p_1=0.79±0.03. As a result, only two parameters

pertaining to indium complexation by carboxylic sites were adjusted to recover the data of **Figure 1** using NICAD, namely the binding parameter $\overline{K}_{In,1}$ and the stoichiometry parameter $n_{In,1}$.

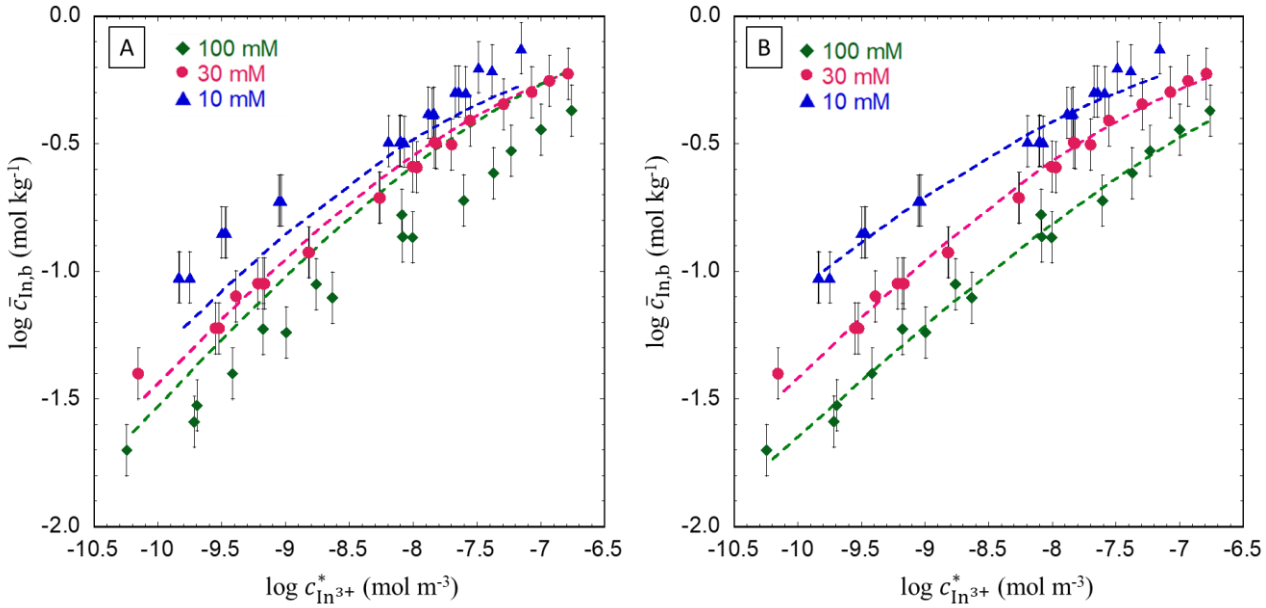

Figure 5: Experimental data (symbols) for indium binding to HNP at three $NaClO_4$ electrolyte concentrations (10mM, 30mM and 100mM) and outcome from NICA-Donnan modelling (dotted lines) when data collected at the three electrolyte concentrations are simultaneously considered for the fitting (A) and when they are considered separately (B). See section C of the supporting materials for more details on the computation of the In-HNP concentrations.

As shown in **Figure 5A**, NICAD approach fails to reproduce the dependence of $\overline{K}_{app}$ on electrolyte concentration and indium-to-reactive sites coverage. Agreement between NICAD and experimental data is achieved only in the case where fitting is performed separately for each electrolyte concentration tested (Figure 5B). The latter fitting procedure, however, leads to strong and inconsistent variations in the values of $\overline{K}_{In,1}$ and $n_{In,1}$ obtained over the whole range of $NaClO_4$ concentration. In turn, such $\overline{K}_{In,1}$ cannot be considered as the intrinsic chemical component of the stability constant of indium-HNPs complexes as it significantly varies with electrolyte concentration, *i.e.* with the extent to which electrostatics impacts on indium binding. A variation in $\overline{K}_{In,1}$ of up to one order magnitude is obtained from NICAD modelling for electrolyte concentrations ranging from 10mM to 100mM with corresponding $\log\overline{K}_{In,1}$ ranging from 4.5 to 5.5, while values of $n_{In,1}$ remains basically constant within experimental error ($n_{In,1}$ = 0.44, 0.51 and 0.45 at 10mM, 30mM and 100 mM electrolyte concentration, respectively).

The failure of NICAD model to properly interpret our In-HNP complexation data is due to theimplementation of Donnan electrostatics to represent the bell-shaped electrostatic potential profiles within and outside nanoparticles defined by κr_p of the order unity. This inadequacy of NICAD model to interpret metal complexation by nanoparticulate systems is masked when data analysis is *not* performed simultaneously over a large range of electrolyte concentrations (as it should). Then,

matching with experiments can be artificially performed but at the cost of physically inconsistent change of $\log\overline{K}_{\mathrm{In},1}$ with salt concentration. Classically, the analysis of metal complexation by nanoparticulate ligands is reported *versus* pH at a *single* electrolyte concentration value in order to examine the competition between protons and metals in their binding to reactive sites. This strategy has thus inevitably masked the inconsistent Donnan electrostatic representation subsumed in NICAD but inadequate for nanoparticles in the thick double layer regime in line with κr_{p} values that do not well exceed unity. The shortcomings of NICAD as formulated here for indium-humics complexation supports the ones evidenced for the binding of protons [25] and divalent metal ions [5,20] to nanoparticulate fulvics and humics.

CONCLUSIONS

The current study demonstrates the correctness in applying the approach by Town *et al*.[5] adopted so far for divalent metal-fulvics/humics complexation and extended here to the binding of trivalent metal species to nanoparticulate humics. Analysis calls for a proper account of both the electrostatic and intrinsic chemical contributions to the measured (apparent) stability of indium-humics complexes, a step that is necessary to subsequently derive the chemodynamics and (bio)availability of these complexes in the vicinity of a reactive macro-interface like an electrode or a microorganism [7,9]. Obviously, the molecular environment of the coordination bond between the metal and the humics/fulvics reactive sites requires further investigations with help of techniques like Extended X-Ray Absorption Fine Structure (EXAFS), which however requires generally rather high metal-to-particle reactive sites coverage, far from the low metal coverage range that prevails under realistic environmental conditions. The Poisson-Boltzmann formalism previously reported by Duval *et al.*[26], where the impact of counterion accumulation at/within the particle surface/body during equilibration with surrounding ionic atmosphere is shown to describe consistently how the apparent stability of indium-humics complexes, depends on electrolyte concentration. The analysis further requires a single adjustable parameter (the radius *R* of the counterions accumulation sphere) pending the protolytic features of the particles are independently determined by consistent analysis of proton titration curves. We further demonstrate and explain the failure of the conventional NICAD model to reproduce our complete set of indium-HNPs complexation data collected at different solution ionic strengths, which echoes previous criticisms of NICAD when applied to model the binding of protons and divalent metal cations to nanoparticles for which Donnan electrostatic representation is clearly inappropriate [5,19,25]. This finding should be a source of concerns because Donnan electrostatic representation is abundantly adopted in various generic thermodynamic models on metal-to-nanoparticulate organic matter complexation [17][42]. Applying these models to nanoparticles in the thick double layer regime inherently bias evaluation of the intraparticulate speciation of indium with humics as they

underestimate the electrostatic contribution, and thus, arbitrarily overestimate the chemical binding component so as to match experimental data at a given solution ionic strength.

Acknowledgments. This work was supported by the French National Research Agency through the national program "Investissements d'Avenir" with the reference ANR-10-LABX-21-01 / LABEX RESSOURCES21. This work was carried out in the Pôle de compétences Physico-Chimie de l'Environnement, LIEC laboratory UMR 7360 CNRS – Université de Lorraine. We acknowledge the contributions of Yves Waldvogel (University of Lorraine), Paco Iglesias (Student of the University of Lorraine) and Pepita Pla-Vilanova (Lleida University, Spain) for preliminary AGNES measurements of indium in the suspensions of nanoparticulate humics.

Supporting Material content.
A. Details on the preparation of the thin mercury film (working electrode).
B. Stability constants of $In(OH)^{2+}$ and $In(OH)_2^+$.
C. Comparison of In-HNP stability constants derived from approximate NICA-Donnan approach and from PB-based formalism (this work).

CRediT author statement

Elise Rotureau: Conceptualization; Data curation; Formal analysis; Funding acquisition; Investigation; Methodology; Validation; Visualization; Writing - original draft; review & editing. **José Paulo Pinheiro**: Conceptualization; Formal analysis; Methodology; Validation; Visualization; Writing - original draft. **Jérôme F.L. Duval:** Conceptualization; Software; Supervision; Validation; Visualization; Writing - original draft

References

[1] J. Buffle, Complexation reactions in aquatic systems: an analytical approach, E. Horwood, Chichester, 1988.
[2] R. M. Town, H.P. van Leeuwen, Intraparticulate speciation analysis of soft nanoparticulate metal complexes. The impact of electric condensation on the binding of Cd 2+ /Pb 2+ /Cu 2+ by humic acids, Physical Chemistry Chemical Physics. 18 (2016) 10049–10058. https://doi.org/10.1039/C6CP01229A.
[3] R. M. Town, H.P. van Leeuwen, Metal ion–humic acid nanoparticle interactions: role of both complexation and condensation mechanisms, Physical Chemistry Chemical Physics. 18 (2016) 18024–18032. https://doi.org/10.1039/C6CP02634F.
[4] H.P. van Leeuwen, R.M. Town, Electric condensation of divalent counterions by humic acid nanoparticles, Environ. Chem. 13 (2015) 76–83. https://doi.org/10.1071/EN15055.
[5] R.M. Town, J.F.L. Duval, H.P. van Leeuwen, The Intrinsic Stability of Metal Ion Complexes with Nanoparticulate Fulvic Acids, Environ. Sci. Technol. 52 (2018) 11682–11690. https://doi.org/10.1021/acs.est.8b02896.
[6] R.M. Town, H.P. van Leeuwen, J. Buffle, Chemodynamics of Soft Nanoparticulate Complexes: Cu(II) and Ni(II) Complexes with Fulvic Acids and Aquatic Humic Acids, Environ. Sci. Technol. 46 (2012) 10487–10498. https://doi.org/10.1021/es3018013.

[7] H.P. van Leeuwen, J.F.L. Duval, J.P. Pinheiro, R. Blust, R.M. Town, Chemodynamics and bioavailability of metal ion complexes with nanoparticles in aqueous media, Environmental Science: Nano. 4 (2017) 2108–2133. https://doi.org/10.1039/c7en00625j.
[8] R.M. Town, J.F.L. Duval, J. Buffle, H.P. van Leeuwen, Chemodynamics of Metal Complexation by Natural Soft Colloids: Cu(II) Binding by Humic Acid, J. Phys. Chem. A. 116 (2012) 6489–6496. https://doi.org/10.1021/jp212226j.
[9] J.F.L. Duval, R.M. Town, H.P. van Leeuwen, Lability of Nanoparticulate Metal Complexes at a Macroscopic Metal Responsive (Bio)interface: Expression and Asymptotic Scaling Laws, The Journal of Physical Chemistry C. 122 (2018) 6052–6065. https://doi.org/10.1021/acs.jpcc.7b11982.
[10] J.F.L. Duval, R.M. Présent, E. Rotureau, Kinetic and thermodynamic determinants of trace metal partitioning at biointerphases: the role of intracellular speciation dynamics, Phys. Chem. Chem. Phys. 18 (2016) 30415–30435. https://doi.org/10.1039/C6CP05717A.
[11] H.P. van Leeuwen, J. Buffle, Chemodynamics of Aquatic Metal Complexes: From Small Ligands to Colloids, Environ. Sci. Technol. 43 (2009) 7175–7183. https://doi.org/10.1021/es900894h.
[12] J.F.L. Duval, Chemodynamics of metal ion complexation by charged nanoparticles: a dimensionless rationale for soft, core–shell and hard particle types, Phys. Chem. Chem. Phys. 19 (2017) 11802–11815. https://doi.org/10.1039/C7CP01750B.
[13] H.P. van Leeuwen, R.M. Town, J. Buffle, Chemodynamics of Soft Nanoparticulate Metal Complexes in Aqueous Media: Basic Theory for Spherical Particles with Homogeneous Spatial Distributions of Sites and Charges, Langmuir. 27 (2011) 4514–4519. https://doi.org/10.1021/la200265p.
[14] R.M. Town, J. Buffle, J.F.L. Duval, H.P. van Leeuwen, Chemodynamics of soft charged nanoparticles in aquatic media: fundamental concepts, J Phys Chem A. 117 (2013) 7643–7654. https://doi.org/10.1021/jp4044368.
[15] D.G. Kinniburgh, C.J. Milne, M.F. Benedetti, J.P. Pinheiro, J. Filius, L.K. Koopal, W.H. Van Riemsdijk, Metal Ion Binding by Humic Acid: Application of the NICA-Donnan Model, Environ. Sci. Technol. 30 (1996) 1687–1698. https://doi.org/10.1021/es950695h.
[16] C.J. Milne, D.G. Kinniburgh, W.H. van Riemsdijk, E. Tipping, Generic NICA−Donnan Model Parameters for Metal-Ion Binding by Humic Substances, Environ. Sci. Technol. 37 (2003) 958–971. https://doi.org/10.1021/es0258879.
[17] E. Tipping, WHAMC—A chemical equilibrium model and computer code for waters, sediments, and soils incorporating a discrete site/electrostatic model of ion-binding by humic substances, Computers & Geosciences. 20 (1994) 973–1023. https://doi.org/10.1016/0098-3004(94)90038-8.
[18] E. Tipping, Humic Ion-Binding Model VI: An Improved Description of the Interactions of Protons and Metal Ions with Humic Substances, Aquatic Geochemistry. 4 (1998) 3–47. https://doi.org/10.1023/A:1009627214459.
[19] R.M. Town, H.P. van Leeuwen, J.F.L. Duval, Rigorous Physicochemical Framework for Metal Ion Binding by Aqueous Nanoparticulate Humic Substances: Implications for Speciation Modeling by the NICA-Donnan and WHAM Codes, Environ. Sci. Technol. 53 (2019) 8516–8532. https://doi.org/10.1021/acs.est.9b00624.
[20] R.M. Town, H.P. van Leeuwen, Intraparticulate Metal Speciation Analysis of Soft Complexing Nanoparticles. The Intrinsic Chemical Heterogeneity of Metal-Humic Acid Complexes, J Phys Chem A. 120 (2016) 8637–8644. https://doi.org/10.1021/acs.jpca.6b08543.

[21] R.M. Town, H.P. van Leeuwen, Dynamic speciation analysis of heterogeneous metal complexes with natural ligands by stripping chronopotentiometry at scanned deposition potential(SSCP), Australian Journal of Chemistry. 57 (2004) 983–992.
[22] J.F.L. Duval, Metal Speciation Dynamics in Soft Colloidal Ligand Suspensions. Electrostatic and Site Distribution Aspects, J. Phys. Chem. A. 113 (2009) 2275–2293. https://doi.org/10.1021/jp809764h.
[23] E. Rotureau, Y. Waldvogel, J.P. Pinheiro, J.P.S. Farinha, I. Bihannic, R.M. Présent, J.F.L. Duval, Structural effects of soft nanoparticulate ligands on trace metal complexation thermodynamics, Phys. Chem. Chem. Phys. 18 (2016) 31711–31724. https://doi.org/10.1039/C6CP06880D.
[24] J.R.S. Martin, I. Bihannic, C. Santos, J.P.S. Farinha, B. Demé, F.A.M. Leermakers, J.P. Pinheiro, E. Rotureau, J.F.L. Duval, Structure of Multiresponsive Brush-Decorated Nanoparticles: A Combined Electrokinetic, DLS, and SANS Study, Langmuir. 31 (2015) 4779–4790. https://doi.org/10.1021/acs.langmuir.5b00530.
[25] J.P. Pinheiro, E. Rotureau, J.F.L. Duval, Addressing the electrostatic component of protons binding to aquatic nanoparticles beyond the Non-Ideal Competitive Adsorption (NICA)-Donnan level: Theory and application to analysis of proton titration data for humic matter, Journal of Colloid and Interface Science. 583 (2021) 642–651. https://doi.org/10.1016/j.jcis.2020.09.059.
[26] J.F.L. Duval, R.M. Town, H.P. van Leeuwen, Poisson–Boltzmann Electrostatics and Ionic Partition Equilibration of Charged Nanoparticles in Aqueous Media, The Journal of Physical Chemistry C. 122 (2018) 17328–17337. https://doi.org/10.1021/acs.jpcc.8b05168.
[27] G.S. Manning, Limiting laws and counterion condensation in polyelectrolyte solutions: IV. The approach to the limit and the extraordinary stability of the charge fraction, Biophysical Chemistry. 7 (1977) 95–102. https://doi.org/10.1016/0301-4622(77)80002-1.
[28] S.A. Wood, I.M. Samson, The aqueous geochemistry of gallium, germanium, indium and scandium, Ore Geology Reviews. 28 (2006) 57–102. https://doi.org/10.1016/j.oregeorev.2003.06.002.
[29] S.L. Thompson, F.C.R. Manning, S.M. McColl, Comparison of the Toxicity of Chromium III and Chromium VI to Cyanobacteria, Bull. Environ. Contam. Toxicol. 69 (2002) 286–293. https://doi.org/10.1007/s00128-002-0059-9.
[30] J.P. Gustafsson, I. Persson, A.G. Oromieh, J.W.J. van Schaik, C. Sjöstedt, D.B. Kleja, Chromium(III) Complexation to Natural Organic Matter: Mechanisms and Modeling, Environ. Sci. Technol. 48 (2014) 1753–1761. https://doi.org/10.1021/es404557e.
[31] E. Tipping, C. Rey-Castro, S.E. Bryan, J. Hamilton-Taylor, Al(III) and Fe(III) binding by humic substances in freshwaters, and implications for trace metal speciation, Geochimica et Cosmochimica Acta. 66 (2002) 3211–3224. https://doi.org/10.1016/S0016-7037(02)00930-4.
[32] L. Marang, P.E. Reiller, S. Eidner, M.U. Kumke, M.F. Benedetti, Combining Spectroscopic and Potentiometric Approaches to Characterize Competitive Binding to Humic Substances, Environ. Sci. Technol. 42 (2008) 5094–5098. https://doi.org/10.1021/es702858p.
[33] A.J. Downs, Chemistry of aluminium, gallium, indium, and thallium, Blackie Academic & Professional, 1993. http://agris.fao.org/agris-search/search.do?recordID=US201300732561 (accessed June 28, 2019).
[34] E. Rotureau, P. Pla-Vilanova, J. Galceran, E. Companys, J.P. Pinheiro, Towards improving the electroanalytical speciation analysis of indium, Analytica Chimica Acta. 1052 (2019) 57–64. https://doi.org/10.1016/j.aca.2018.11.061.

[35] J. Galceran, E. Companys, J. Puy, J.P. Pinheiro, E. Rotureau, AGNES in irreversible systems: the indium case, Journal of Electroanalytical Chemistry. 901 (2021) 115750. https://doi.org/10.1016/j.jelechem.2021.115750.
[36] J. Galceran, E. Companys, J. Puy, J. Cecilia, J.L. Garces, AGNES: a new electroanalytical technique for measuring free metal ion concentration, Journal of Electroanalytical Chemistry. 566 (2004) 95–109. https://doi.org/10.1016/j.jelechem.2003.11.017.
[37] E.M. Thurman, R.L. Malcolm, Preparative isolation of aquatic humic substances, Environ. Sci. Technol. 15 (1981) 463–466. https://doi.org/10.1021/es00086a012.
[38] W.G. Botero, M. Pineau, N. Janot, R.F. Domingos, J. Mariano, L.S. Rocha, J.E. Groenenberg, M.F. Benedetti, J.P. Pinheiro, Isolation and purification treatments change the metal-binding properties of humic acids: effect of HF/HCl treatment, Environ. Chem. 14 (2018) 417–424. https://doi.org/10.1071/EN17129.
[39] M.H. Tehrani, E. Companys, A. Dago, J. Puy, J. Galceran, Free indium concentration determined with AGNES, Science of The Total Environment. 612 (2018) 269–275. https://doi.org/10.1016/j.scitotenv.2017.08.200.
[40] J.P. Gustafsson, Visual MINTEQ version 3.0. KTH, Department of Land and Water Resources Engineering, Stockolm, Sweden, 2009. Available at http://vminteq.lwr.kth.se/, (n.d.).
[41] J.F.L. Duval, H. Ohshima, Electrophoresis of Diffuse Soft Particles, Langmuir. 22 (2006) 3533–3546. https://doi.org/10.1021/la0528293.
[42] M.F. Benedetti, W.H. Van Riemsdijk, L.K. Koopal, Humic Substances Considered as a Heterogeneous Donnan Gel Phase, Environ. Sci. Technol. 30 (1996) 1805–1813. https://doi.org/10.1021/es950012y.
[43] Y. Takahashi, Y. Minai, S. Ambe, Y. Makide, F. Ambe, T. Tominaga, Simultaneous determination of stability constants of humate complexes with various metal ions using multitracer technique, Science of The Total Environment. 198 (1997) 61–71. https://doi.org/10.1016/S0048-9697(97)05442-9.
[44] J.C. Stern, J.E. Sonke, V.J.M. Salters, A capillary electrophoresis-ICP-MS study of rare earth element complexation by humic acids, Chemical Geology. 246 (2007) 170–180. https://doi.org/10.1016/j.chemgeo.2007.09.008.
[45] J.E. Sonke, V.J.M. Salters, Lanthanide–humic substances complexation. I. Experimental evidence for a lanthanide contraction effect, Geochimica et Cosmochimica Acta. 70 (2006) 1495–1506. https://doi.org/10.1016/j.gca.2005.11.017.